JACS
JOURNAL OF THE AMERICAN CHEMICAL SOCIETY
Communication
pubs.acs.org/JACS

Highly Emissive Covalent Organic Frameworks

Sasanka Dalapati,[†] Enquan Jin,[‡] Matthew Addicoat,[§] Thomas Heine,[§] and Donglin Jiang*[,†]

[†]Field of Energy and Environment, School of Materials Science, Japan Advanced Institute of Science and Technology, 1-1 Asahidai, Nomi 923-1292, Japan

[‡]Department of Structural Molecular Science, School of Physical Science, SOKENDAI, Hayama, Kanagawa 240-0193, Japan

[§]Wilhelm-Ostwald-Institut für Physikalische und Theoretische Chemie, Universität Leipzig, Linnéstrasse 2, 04103 Leipzig, Germany

Supporting Information

ABSTRACT: Highly luminescent covalent organic frameworks (COFs) are rarely achieved because of the aggregation-caused quenching (ACQ) of $\pi-\pi$ stacked layers. Here, we report a general strategy to design highly emissive COFs by introducing an aggregation-induced emission (AIE) mechanism. The integration of AIE-active units into the polygon vertices yields crystalline porous COFs with periodic π-stacked columnar AIE arrays. These columnar AIE π-arrays dominate the luminescence of the COFs, achieve exceptional quantum yield via a synergistic structural locking effect of intralayer covalent bonding and interlayer noncovalent $\pi-\pi$ interactions and serve as a highly sensitive sensor to report ammonia down to sub ppm level. Our strategy breaks through the ACQ-based mechanistic limitations of COFs and opens a way to explore highly emissive COF materials.

Covalent organic frameworks (COFs) are a class of crystalline porous polymers that enable the precise integration of organic units into periodic columnar π-arrays and inherent pores, making them useful in various applications.[1−6] The $\pi-\pi$ layered structures easily trigger the thermal decay of photoexcited states and result in less or nonemissive COFs. This aggregation-caused quenching (ACQ) mechanism is ubiquitous for COFs, and this mechanistic limitation is the reason why highly luminescent COFs are rarely achieved[6a−c] even though various luminescent π-units have been employed for the synthesis of COFs.[5c,6d] In this study, we developed a general strategy for designing highly luminescent COFs by introducing aggregation-induced emission (AIE) mechanism to the π-frameworks in which the intralayer covalent link and interlayer noncovalent π-interaction work synergistically to impede the rotation-induced energy dissipation.

AIE is a phenomenon that chromophores become emissive in aggregated states and has shown broad applications in light-emitting diodes, light-harvesting, photonic devices, chemosensing, and bioimaging.[7] Although porous polymers with AIE building units have been reported,[8,9] none of them consist of π-stacked ordering structures. The synthesis of AIE-based COFs that satisfy the requirements of π-ordering, porosity, and high luminescence is important to the advancement of AIE materials. However, AIE-based COFs and their functions are unprecedented.

We designed an AIE-active tetraphenylethene (TPE) unit for the synthesis of a highly emissive two-dimensional COF (Scheme 1, TPE-Ph COF; Supporting Information (SI); Figures S1−S5). Solvothermal condensation of TPE-cored boronic acids (TPEBA) and 1,2,4,5-tetrahydroxybenzene (THB) in a mixture of dioxane/mesitylene (1/1 by vol.) at 90 °C for 3 days yielded light yellow crystallites in 71% isolated

Scheme 1. Schematic Representation for the Synthesis of TPE-Ph COF with TPE Units at the Vertices of the Dual-Pore Kagome Lattice

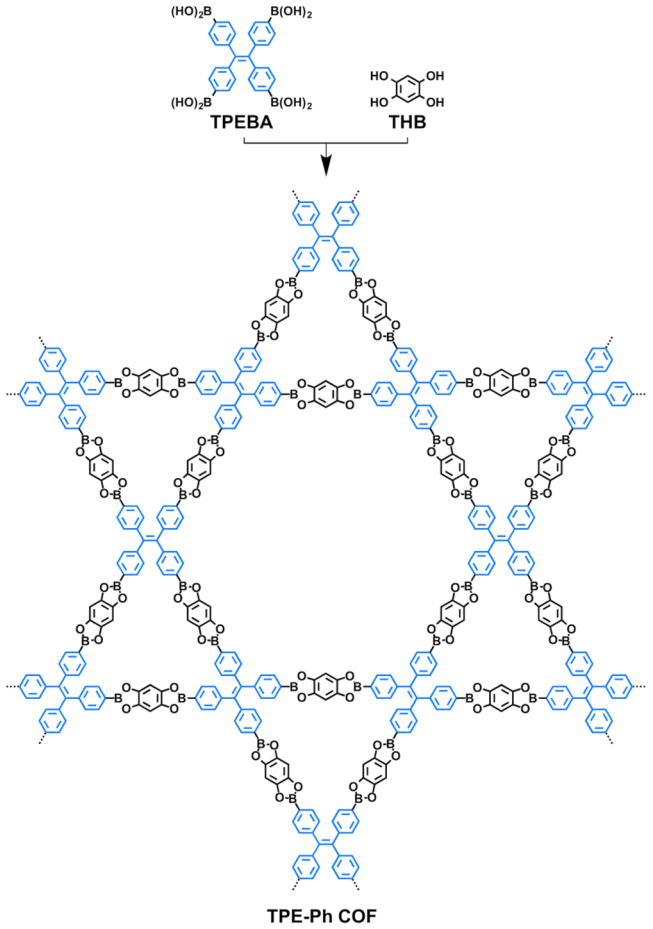

Received: March 14, 2016
Published: April 24, 2016

DOI: 10.1021/jacs.6b02700
J. Am. Chem. Soc. 2016, 138, 5797−5800

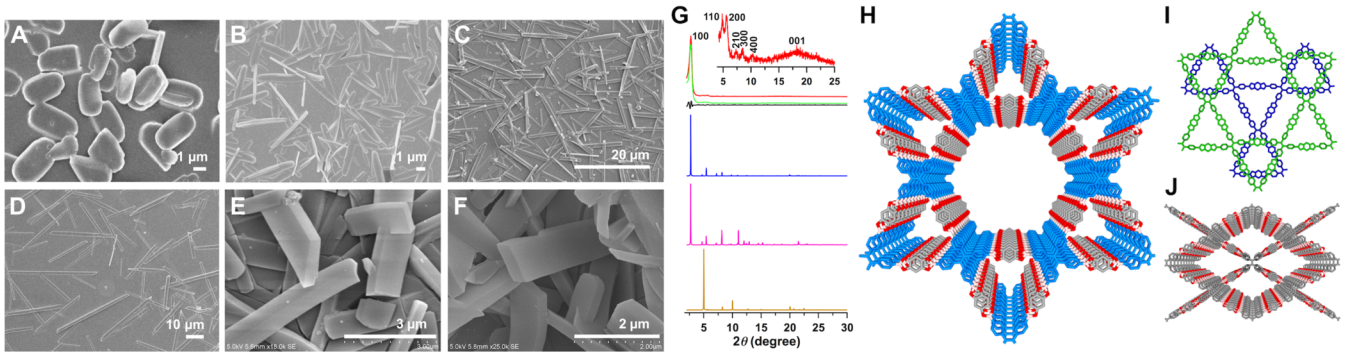

Figure 1. FE-SEM images of the TPE-Ph COF samples prepared at different reaction times of (A) 3 days, (B) 10 days, (C) 20 days, and (D) 30 days. High-resolution SEM images of the TPE-Ph COF samples prepared at different times of (E) 20 days and (F) 30 days. (G) PXRD patterns of TPE-Ph COF (experimentally observed (red), Pawley refined (green), difference between experimental and Pawley refined data (black), calculated for the AA-stacking mode of dual-pore Kagome structure (blue), AB-stacking mode of dual-pore Kagome structure (pink), and AA-stacking mode of single-pore rhombic structure (orange)). Crystal structures of the dual-pore Kagome TPE-Ph COF in (H) AA and (I) AB stacking modes, and (J) single-pore rhombic AA stacking mode.

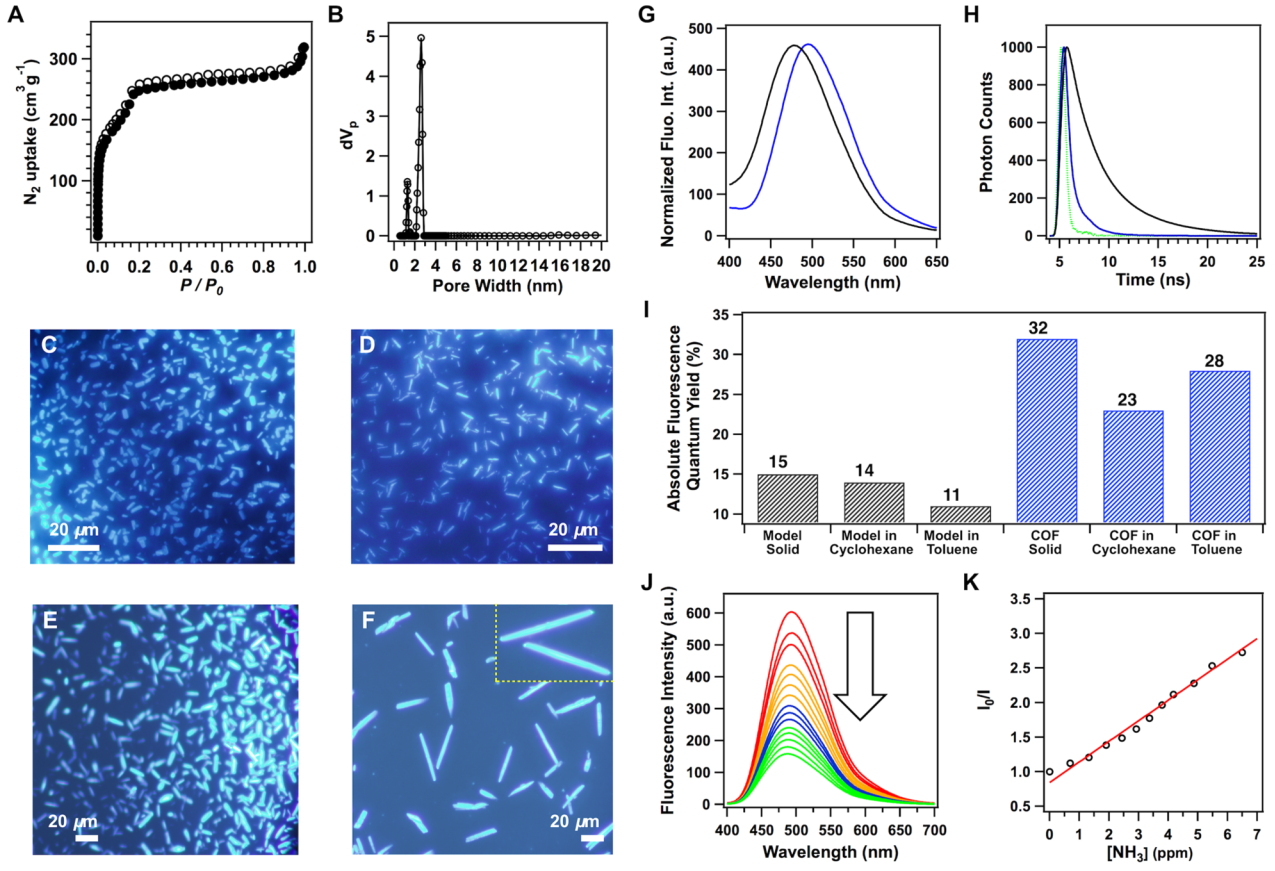

Figure 2. (A) N_2 adsorption (●) and desorption (○) isotherm curves and (B) pore size distribution profiles of the TPE-Ph COF. Fluorescence microscopy images of TPE-Ph COF samples prepared at different reaction times of (C) 3 days, (D) 10 days, (E) 20 days, and (F) 30 days (the yellow rectangle contains an inset image showing an enlarged view of the belts). (G) Fluorescence spectra and (H) lifetime profile of the TPE model compound (black) and the TPE-Ph COF (blue). The green curve in (H) is the instrument response function. (I) Fluorescence quantum yield of the TPE-Ph COF compared to the model compound. (J) Fluorescence spectral change of the TPE-Ph COF upon addition of ammonia. (K) Stern–Volmer plot of the fluorescence quenching by ammonia.

yield (SI). Field-emission scanning electron microscopy (FE-SEM) revealed that TPE-Ph COF has rectangular belts and sharp faces, edges, and corners (Figure 1A–F). These well-defined morphologies encouraged us to monitor the time-dependent growth of the TEP-Ph COF crystallites. The belt length was approximately 4 μm on average for the COF samples after three-day reaction (Figure 1A). When the reaction time was extended to 10 days, the belts extended to 6 μm (Figure 1B) while decreasing their width to nearly 1 μm. We further extended the reaction time to 20 and 30 days and observed that the belts further increased to 16 and 53 μm, respectively (Figures 1C–F). These changes show that the COF belts grow while maintaining rectangular shapes with clear

DOI: 10.1021/jacs.6b02700
J. Am. Chem. Soc. 2016, 138, 5797–5800

faces, edges, and corners. The TPE-Ph COF is stable up to 400 °C under nitrogen atmosphere (Figure S6).

The TPE-Ph COF exhibited strong diffraction signals at 2.74°, 4.82°, 5.58°, 7.28°, 8.54°, 10.30°, and 18.52°, which were assigned to be 100, 110, 200, 210, 300, 400, and 001 facets, respectively (Figure 1G, red curve; for enlarged profile, see Figure S7). Pawley refinements yielded a PXRD pattern (green curve) that well matched with the experimentally observed one, as reflected by their negligible differences (black curve). The lattice parameters were determined as $a = b = 37.466$ Å, $c = 4.45$ Å, $\alpha = \beta = 90°$, and $\gamma = 120°$ (SI). Density functional-based tight binding (DFTB) calculations[10] revealed a dual-pore Kagome lattice and a single-pore rhombic lattice with AA and AB stacking modes, respectively (SI). The AA stacking mode (Figure 1H) of the Kagome lattice reproduced the peak position and intensity of the PXRD pattern (Figure 1G, blue curve), whereas the AB stacking mode (pink curve) deviated from the experimentally observed PXRD pattern (Figure 1I). The simulated peak positions of the rhombic lattice (Figure 1J) were completely different (Figure 1G, orange curve) from the experimentally observed PXRD pattern. Thus, the TPE units are located at the vertices and the phenyl linkers occupy at the edges of the polygons to form periodic columnar TPE π-arrays and a dual-pore Kagome lattice with trigonal micropores and hexagonal mesopores.

Nitrogen sorption measurements were conducted at 77 K to evaluate the porosity. The sorption curves were classified as a combination of typical type I and IV isotherms, which are characteristic of micropores and mesopores, respectively (Figure 2A). The Brunauer–Emmett–Teller (BET) surface area and pore volume were estimated to be 962 $m^2 g^{-1}$ and 0.5 $cm^3 g^{-1}$, respectively. Theoretical surface area for the AA-stacked TPE-Ph COF (Figure S8) was calculated to be 1005 $m^2 g^{-1}$, which is close to experimental value. The pore size distribution was evaluated using the nonlocal density functional theory, and the pore sizes were calculated to be 1.3 and 2.6 nm (Figure 2B), which are attributed to the micropores and mesopores, respectively. Both crystal structure and nitrogen sorption analysis suggest a dual-pore Kagome lattice for the TPE-Ph COF.

Figures 2C–F shows the fluorescence microscope images of the TPE-Ph COF samples prepared after 3-, 10-, 20-, and 30-day reactions. Surprisingly, all the TPE-Ph COF samples exhibited brilliant luminescence in the same color, irrespective of the reaction time. More interestingly, each belt was highly luminescent and the luminescence was homogeneously observed across the whole belt (Figure 2F, inset). These results indicate that the structural growth does not alter the luminescent function of TPE-Ph COF.

The TPE model compound exhibited an absorption band at 385 nm, whereas that of the TPE-Ph COF exhibited a peak centered at 390 nm (Figure S9). Upon excitation, the solid samples of the TPE model compound and TPE-Ph COF emitted brilliant blue luminescence, with peak maxima at 480 and 500 nm, respectively (Figure 2G). The absolute fluorescence quantum yield of the TPE-Ph COF solid samples was observed to be as high as 32%, whereas the solid samples of the TPE model compound exhibited an absolute quantum yield of 15% (Figure 2I). Compared to the model compound, the TPE-Ph COF exhibited 2- to 3-fold high luminescence quantum yields (Figure 2I). This enhancement in the solid state suggests that the π–π interactions between layers of COFs additionally contribute to the higher fluorescence quantum yield. Time-resolved fluorescence spectroscopy revealed that the lifetimes of the model compound and TPE-Ph COF were 3.8 and 0.7 ns, respectively (Figure 2H). By combining the lifetime and quantum yield, we evaluated the radiative rate constant to be 4.6×10^8 s^{-1}, which was 3.9×10^7 s^{-1} for the model compound. These results indicate that the TPE-Ph COF facilitates the radiative process, leading to a rate constant 1 order of magnitude greater than the model compound.

DFTB calculations of the TPE vertex analogue, COF monolayer, and AA stacked COF support the existence of the structural effects. The phenyl rings in the COF monolayer require a rotation energy of 9.9 kcal mol^{-1} (at 70° dihedral angle), which is higher than that (7.1 kcal mol^{-1}) of the TPE vertex analogue (Figures S10 and S11). By contrast, for the layered TPE-Ph COF, this barrier was as high as 216.7 kcal mol^{-1} (Figure S12). Further enhancement of the dihedral angle to greater than 70° drastically increased the rotation barrier energy for the layered TPE-Ph COF, whereas the barriers were hardly changed for the vertex analogue and the monolayer (Figures S10–S12). At the monolayer level, the four phenyl groups of the TPE vertices are connected to four different linkers that substantially decrease the free rotation of the phenyl groups. At the layered framework level of the TPE-Ph COF, the π–π stacking further restricts the rotation of the four phenyl groups.[7] Therefore, the structural synergies, i.e., the intralayer covalent bond and interlayer noncovalent packing, work together to prevent the excited state distortion,[9b] and hence the excited energy immediately releases via fluorescence decay. The above structural insights explain why the quantum yield of the TPE-Ph COF is much higher than that of the TPE model compound. To the best of our knowledge, the TPE-Ph COF exhibits the highest luminescence quantum yield of the COFs reported to date.

Boronate linkages of the TPE-Ph COF form Lewis acid–base pair when interacted with ammonia because boronate serves as Lewis acid and ammonia is a Lewis base.[1c] Based on this Lewis acid–base interaction, we explored the TPE-Ph COF as a highly sensitive fluorescence sensor for ammonia. Indeed, upon addition of ammonia, the TPE-Ph COF (2 mg of COF in 2 mL of toluene) exhibited a rapid response to ammonia and decreased its luminescence (Figure 2J). Stern–Volmer plot revealed an almost linear curve, whereas the fluorescence quenching rate constant k_q ($= k_{SV}/\tau$) was evaluated to be as high as 4.1×10^{14} M^{-1} s^{-1} (Figure 2K). We can further decrease the amount of COF to 0.25 mg (2 mL toluene) for the detection of ammonia. In this case, 1 ppm ammonia could lead to 30% down of fluorescence intensity (Figure S13), leading to a k_q value of 6.3×10^{14} M^{-1} s^{-1}. This ammonia sensing was also observed in cyclohexane, whereas the k_q value was 1.4×10^{14} M^{-1} s^{-1} (Figure S14). These extremely high k_q values suggest that the TPE-Ph COF is a highly sensitive ammonia detector at sub ppm level.

In summary, we have developed a novel way to highly emissive COFs by exploring aggregation-induced emission mechanisms for structural design. Integrating TPE units into the vertices of the COFs significantly reduces the rotation-induced excitation-energy dissipation and reveals a synergistic structural locking effect originating from the covalent bonding and noncovalent π–π interactions. This discovery could lead to a new generation of highly luminescent COF materials that retain high quantum yields in both solid and solutions and function as highly sensitive sensor to detect specific chemicals.

DOI: 10.1021/jacs.6b02700
J. Am. Chem. Soc. 2016, 138, 5797–5800

Our AIE-based concept breaks through ACQ-related mechanistic limitations of COFs and offers a platform for exploring highly ordered yet emissive framework materials. We anticipate that the high luminescence together with the confined porous structure will be useful in sensing, imaging, and lasing applications.

■ ASSOCIATED CONTENT

Supporting Information

The Supporting Information is available free of charge on the ACS Publications website at DOI: 10.1021/jacs.6b02700.

Materials and methods, syntheses and characterizations, Tables S1 and S2, and Figures S1−S14 (PDF)

■ AUTHOR INFORMATION

Corresponding Author

*djiang@jaist.ac.jp

Notes

The authors declare no competing financial interest.

■ ACKNOWLEDGMENTS

S.D. is an International Research Fellow of the Japan Society for the Promotion of Science (JSPS).

■ REFERENCES

(1) (a) Feng, X.; Ding, X.; Jiang, D. *Chem. Soc. Rev.* **2012**, *41*, 6010−6022. (b) Côté, A. P.; Benin, A. I.; Ockwig, N. W.; Matzger, A. J.; O'Keeffe, M.; Yaghi, O. M. *Science* **2005**, *310*, 1166−1170. (c) Doonan, C. J.; Tranchemontagne, D. J.; Glover, T. G.; Hunt, J. R.; Yaghi, O. M. *Nat. Chem.* **2010**, *2*, 235−238. (d) Waller, P. J.; Gandara, F.; Yaghi, O. M. *Acc. Chem. Res.* **2015**, *48*, 3053−3063. (e) Liu, Y.; Ma, Y.; Zhao, Y.; Sun, X.; Gándara, F.; Furukawa, H.; Liu, Z.; Zhu, H.; Zhu, C.; Suenaga, K.; Oleynikov, P.; Alshammari, A. S.; Zhang, X.; Terasaki, O.; Yaghi, O. M. *Science* **2016**, *351*, 365−369.

(2) (a) Ding, X.; Chen, L.; Honso, Y.; Feng, X.; Saengsawang, O.; Guo, J. D.; Saeki, A.; Seki, S.; Irle, S.; Nagase, S.; Parasuk, V.; Jiang, D. *J. Am. Chem. Soc.* **2011**, *133*, 14510−14513. (b) Feng, X.; Liu, L.; Honsho, Y.; Saeki, A.; Seki, S.; Irle, S.; Dong, Y. P.; Nagai, A.; Jiang, D. *Angew. Chem., Int. Ed.* **2012**, *51*, 2618−2622. (c) Dalapati, S.; Addicoat, M.; Jin, S.; Sakurai, T.; Gao, J.; Xu, H.; Irle, S.; Seki, S.; Jiang, D. *Nat. Commun.* **2015**, *6*, 7786. (d) Xu, H.; Gao, J.; Jiang, D. *Nat. Chem.* **2015**, *7*, 905−912.

(3) (a) Smith, B. J.; Dichtel, W. R. *J. Am. Chem. Soc.* **2014**, *136*, 8783−8789. (b) Spitler, E. L.; Dichtel, W. R. *Nat. Chem.* **2010**, *2*, 672−677. (c) Colson, J. W.; Woll, A. R.; Mukherjee, A.; Levendorf, M. P.; Spitler, E. L.; Shields, V. B.; Spencer, M. G.; Park, J.; Dichtel, W. R. *Science* **2011**, *332*, 228−231. (d) Spitler, E. L.; Koo, B. T.; Novotney, J. L.; Colson, J. W.; Uribe-Romo, F. J.; Gutierrez, G. D.; Clancy, P.; Dichtel, W. R. *J. Am. Chem. Soc.* **2011**, *133*, 19416−19421.

(4) (a) Dogru, M.; Handloser, M.; Auras, F.; Kunz, T.; Medina, D.; Hartschuh, A.; Knochei, P.; Bein, T. *Angew. Chem., Int. Ed.* **2013**, *52*, 2920−2924. (b) Ding, S. Y.; Gao, J.; Wang, Q.; Zhang, Y.; Song, W. G.; Su, C. Y.; Wang, W. *J. Am. Chem. Soc.* **2011**, *133*, 19816−19822. (c) Biswal, B. P.; Chandra, S.; Kandambeth, S.; Lukose, B.; Heine, T.; Banerjee, R. *J. Am. Chem. Soc.* **2013**, *135*, 5328−5331. (d) Ren, S.; Bojdys, M. J.; Dawson, R.; Laybourn, A.; Khimyak, Y. Z.; Adams, D. J.; Cooper, A. I. *Adv. Mater.* **2012**, *24*, 2357−2361. (e) Kuhn, P.; Antonietti, M.; Thomas, A. *Angew. Chem., Int. Ed.* **2008**, *47*, 3450−3453.

(5) (a) Jackson, K. T.; Reich, T. E.; El-Kaderi, H. M. *Chem. Commun.* **2012**, *48*, 8823−8825. (b) Fang, Q.; Zhuang, Z.; Gu, S.; Kaspar, R. B.; Zheng, J.; Wang, J.; Qiu, S.; Yan, Y. *Nat. Commun.* **2014**, *5*, 4503. (c) Zhou, T.-Y.; Xu, S.-Q.; Wen, Q.; Pang, Z.-F.; Zhao, X. *J. Am. Chem. Soc.* **2014**, *136*, 15885−15888. (d) Vyas, V. S.; Haase, F.; Stegbauer, L.; Savasci, G.; Podjaski, F.; Ochsenfeld, C.; Lotsch, B. V. *Nat. Commun.* **2015**, *6*, 8508. (e) Xu, L.; Zhou, X.; Tian, W. Q.; Gao, T.; Zhang, Y. F.; Lei, S.; Liu, Z. F. *Angew. Chem., Int. Ed.* **2014**, *53*, 9564−9568. (g) Zhu, Y.; Wan, S.; Jin, Y.; Zhang, W. *J. Am. Chem. Soc.* **2015**, *137*, 13772−13775.

(6) (a) Wan, S.; Guo, J.; Kim, J.; Ihee, H.; Jiang, D. *Angew. Chem., Int. Ed.* **2008**, *47*, 8826−8830. (b) Wan, S.; Guo, J.; Kim, J.; Ihee, H.; Jiang, D. *Angew. Chem., Int. Ed.* **2009**, *48*, 5439−5442. (c) Dalapati, S.; Jin, S.; Gao, J.; Xu, Y.; Nagai, A.; Jiang, D. *J. Am. Chem. Soc.* **2013**, *135*, 17310−17313. (d) Feng, X.; Chen, L.; Honsho, Y.; Saengsawang, O.; Liu, L.; Wang, L.; Saeki, A.; Irle, S.; Seki, S.; Dong, Y. P.; Jiang, D. *Adv. Mater.* **2012**, *24*, 3026−3031.

(7) (a) Luo, J.; Xie, Z.; Lam, J.; Cheng, L.; Chen, H.; Qiu, C.; Kwok, H. S.; Zhan, X.; Liu, Y.; Zhu, D.; Tang, B. Z. *Chem. Commun.* **2001**, 1740−1741. (b) Mei, J.; Leung, N. L. C.; Kwok, R. T. K.; Lam, J. W. Y.; Tang, B. Z. *Chem. Rev.* **2015**, *115*, 11718. (c) Ding, D.; Li, K.; Liu, B.; Tang, B. Z. *Acc. Chem. Res.* **2013**, *46*, 2441−2453. (d) Bracco, S.; Beretta, M.; Cattaneo, A.; Comotti, A.; Falqui, A.; Zhao, K.; Rogers, C.; Sozzani, P. *Angew. Chem., Int. Ed.* **2015**, *54*, 4773−4777.

(8) (a) Xu, Y.; Chen, L.; Guo, Z.; Nagai, A.; Jiang, D. *J. Am. Chem. Soc.* **2011**, *133*, 17622−17625. (b) Gong, Q.; Hu, Z.; Deibert, B. J.; Emge, T. J.; Teat, S. J.; Banerjee, D.; Mussman, B.; Rudd, N. D.; Li, J. *J. Am. Chem. Soc.* **2014**, *136*, 16724−16727.

(9) (a) Shustova, N. B.; McCarthy, B. D.; Dincă, M. *J. Am. Chem. Soc.* **2011**, *133*, 20126−20129. (b) Wei, Z.; Gu, Z.-Y.; Arvapally, R. K.; Chen, Y.-P.; McDougald, R. N., Jr.; Ivy, J. F.; Yakovenko, A. A.; Feng, D.; Omary, M. A.; Zhou, H.-C. *J. Am. Chem. Soc.* **2014**, *136*, 8269−8276. (c) Guo, Y.; Feng, X.; Han, T.; Wang, S.; Lin, Z.; Dong, Y.; Wang, B. *J. Am. Chem. Soc.* **2014**, *136*, 15485−15488.

(10) (a) Accelrys. *Material Studio Release Notes*, Release 4.4; Accelrys Software: San Diego, 2008. (b) Aradi, B.; Hourahine, B.; Frauenheim, T. *J. Phys. Chem. A* **2007**, *111*, 5678−5684. (c) http://www.dftb.org.

DOI: 10.1021/jacs.6b02700
J. Am. Chem. Soc. 2016, 138, 5797−5800